Understanding process-related efficiency variations in mc-Si PERC cells

Sven Wasmer, **Johannes Greulich**, **Hannes Höffler**, **Nico Wöhrle** & **Stefan Rein**, Fraunhofer Institute for Solar Energy Systems ISE, Freiburg, Germany

ABSTRACT
This paper introduces and explains a simulation-assisted approach for determining and ranking the most influential causes of variations in experimentally obtained solar cell efficiencies, using the example of an industrially feasible multicrystalline silicon (mc-Si) passivated emitter and rear cell (PERC) process. With the objectives of being independent of material variations and of analysing process-related impacts only, 51 neighbouring high-performance mc-Si wafers are distributed in an experiment in which more than 800 mc-Si PERC cells in total are processed, and this sub-group is comprehensively characterized. The elevated data serve as input for modelling the resulting distribution of cell efficiencies on the basis of numerical 3D simulations, metamodelling and Monte Carlo runs. In order to understand the most detrimental impacts responsible for a widening of this distribution, a variance-based sensitivity analysis is conducted, where the parameters are ranked according to their impact on the total variance of cell efficiencies. In this case, it is possible to explain over 80% of the measured total variance; moreover, the rear-side passivation and a wrap-around during the emitter etch-back process can be identified as responsible for 80% of the variance. The approach presented is especially helpful for ramping up PERC production; however, since it is basically transferable to any solar cell concept, it can also be applied to optimize established production lines.

Introduction
As of 2014, according to the ITRPV Roadmap [1], almost 90% of the solar cells produced are still based on the conventional concept, namely the solar cell with an aluminium back-surface field (Al-BSF) on the entire rear side. Partly because of the introduction of the so-called *high-performance multi* (HPM) wafers, which allow much higher bulk lifetimes than conventional mc-Si wafers, more and more cell producers are currently switching their production lines to implement the passivated emitter and rear cell (PERC) concept [2], with dielectric passivation layers and local contacting geometries on the rear side. Although this, in principle, permits higher cell efficiencies because of less recombination on the rear side and better light-trapping properties, there are several challenges during the ramping-up phase that have to be dealt with. In this phase, not only the absolute levels of cell efficiencies, which can be analysed, for instance via a loss analysis [3], but also variations thereof have to be considered. An understanding of the causes can reveal the critical processes and parameters that need to be measured more accurately and better tuned, thus leading to an overall improvement in the quality and yield of a production line.

Several works have been published on this topic and will be briefly mentioned here. There are publications dealing with a statistical analysis of wafer process data and cell data: time series analysis and data manipulation methods are used to detect and understand temporal changes in the final cell characteristics [4,5]. A recent publication [6] analyses, using data mining methods, wafer process data and their correlations with the finished cell characteristics of hundreds of thousands of solar cells, and is able to explain large shares of the measured variance with the data acquired during processing.

Alternatively, methods based on numerical solar cell simulations have been presented. These first deal with the modelling and understanding of the distribution of cell efficiencies of an mc Al-BSF process [7], which is later refined by (to the authors' knowledge) the first application of metamodelling and Monte Carlo simulations in PV research [8]. In the most recent work [9], the approach is transferred to the PERC process, and local derivatives of the metamodel are used as a sensitivity measure to detect the most relevant impacts.

In this paper the approaches mentioned above and in a recent publication [10] are followed and enhanced by using state-of-the-art metamodelling. Then, by means of a variance-based sensitivity analysis, the impacts on a measured distribution of cell efficiencies are globally investigated. The approach presented consists of an overview of the models applied for the numerical 3D device simulations using Sentaurus TCAD [11], the modelling of the experimentally achieved distribution of cell efficiencies with Monte Carlo runs. This is followed by a variance-based sensitivity analysis, where the input parameters are ranked according to their impact on the total variance. The approach is demonstrated by an example application to an industrially feasible mc-Si PERC process with laser-fired contacts (LFC, [12]).

Approach
The approach taken here for investigating the impacts of process variations on the distribution of cell efficiencies consists of the following steps:

1. Production and characterization of solar cells.

2. Determination of the relevant input parameters for the simulation, and their distributions.

3. Numerical device simulations and metamodelling thereof.

4. Modelling of the distributions of cell efficiencies via the Monte Carlo method, and validation by measurements.

5. Investigation of the impact of each input parameter in a variance-based sensitivity analysis.

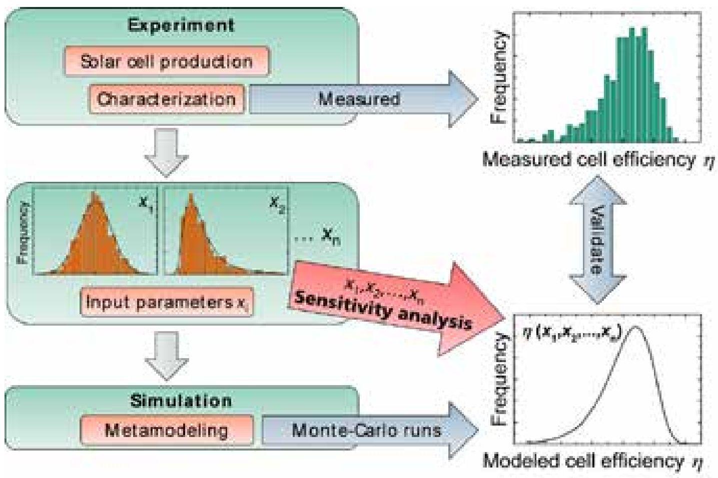

Figure 1. Overview of the approach for investigating the impacts of process variations on the distribution of cell efficiencies. In the experiment, the distributions of the cell efficiencies and of the input parameters for the simulations are determined. Monte Carlo runs of a metamodel of the numerical 3D device simulations are carried out, in order to model the distribution of cell efficiencies, which are then validated by the experimentally obtained efficiencies. The input parameters are ranked according to their influence on the total variance in a variance-based sensitivity analysis.

The approach is shown schematically in Fig. 1 and will be explained in detail next. The first two steps basically serve to compile the prevailing variations of cell efficiencies and parameters in a production line via inline and offline characterization methods, and can be assisted by simulations if necessary. The typical steps are discussed in a later section, but first the focus will be on the simulation-based evaluation (steps 3–5) after the data collection.

The numerical 3D device simulations, which are conducted at a device temperature of 25°C, can be divided into: 1) an optical part, in which the spectrally and spatially resolved generation profiles of charge carriers are calculated; and 2) an electrical part, in which these generation profiles are used as input, and the current-voltage (I–V) curve is computed.

For the optical part, the Monte Carlo ray tracer of a Synopsis Sentaurus Device is used. The front side is modelled on the assumption of thin SiN_x layers of thickness d_{ARC}; these are described by Fresnel's equations using the transfer-matrix formalism [13], on a textured surface, which is described in the case of an isotexture by a characteristic angle $\omega_{texture}$ [14,15]. For the silicon bulk with a substrate thickness of d_{Si}, Lambert-Beer's law [16] is assumed, and the rear side is modelled by the Phong model with parameters R_0 and ω_{Phong} [17]. Later, the shading of the front side metallization is accounted for by scaling the generation current densities j_{ph} by a factor of $(1–M_{met})$, where M_{met} is the optical shading ratio. In this case, variations in j_{ph} largely depend on variations in texture strength $\omega_{texture}$ only, and therefore d_{ARC}, d_{Si}, R_0 and ω_{Phong} are kept constant in the subsequent electrical part of the simulation.

In the electrical simulations of solar cell concepts with structured rear sides, as in the case of PERC, it is convenient to assume an effective front side [18] and to account for the shading of the front metallization by scaling j_{ph} and by considering an external series resistance R_s which contains the area-weighted contributions of the emitter, contact and grid resistances. Furthermore, to account for non-ideal recombination at, for instance, the cell edges or the space charge region, a second diode with ideality $n_2 = 2$ and dark saturation current density j_{02} is added analytically after finishing the numerical Sentaurus Device simulations. The symmetry element applied in the Sentaurus Device usually has a magnitude of d_{Si} in the direction perpendicular to the wafer surface (z axis), and of half the distance between the contacts on the rear side in the other dimensions (x and y axes).

The emitter profile is determined by means of electrochemical capacitance–voltage (ECV) measurements and imported into the Sentaurus Device, leaving an effective surface recombination velocity $S_{eff,front}$ (consisting of a portion $S_{pass,front}$ in the passivated area and a portion $S_{met,front}$ in the metallized area) as a free parameter. The bulk recombination is modelled by a mid-band gap Shockley-Read-Hall (SRH) defect with defect parameters τ_{n0} and τ_{p0}; the recombination at the rear side is modelled by the surface recombination velocities $S_{pass,rear}$ in the passivated area and $S_{met,rear}$ in the metallized area.

The areas of a local rear contact are usually defined via a contacted and a larger recombination-active region. In the case of the LFC approach, the model of a point contact with a recombination-active area (damaged by the laser pulse) with radius r_{LFC} that is twice the size of that of the contacted region $r_{LFC,cont.}$ is used. The model is implemented for the surface recombination velocity $S_{met,rear}$ in the damaged area, introduced by Schwab [19] and applied by Wöhrle et al. [20]. With regard to general models for silicon solar cell simulation, those summarized by Fell et al. [21] are used. For adjusting the density-of-states effective mass of holes for self-consistency of the band gap, effective density of states and intrinsic density at 25°C, the recommendation of Altermatt [22] is followed.

Once the input parameters (e.g. wafer thickness, base doping concentration, texture strength $\omega_{texture}$, emitter doping profile and saturation current density), as well as their minimum and maximum attainable values are known, the next step consists of selecting an adequate experiment design for the numerical simulations, in order to achieve the lowest computation times and the best interpolation properties later. To this end, a space-filling design of experiments (DOE) is chosen, and the design creator available online [23] is utilized for the generation of 300 equidistant sample points in the n-dimensional input space. The results for the four-cell performance characteristics – short-circuit current density j_{sc}, open-circuit voltage V_{oc}, fill factor FF and energy conversion efficiency η – of the numerical device simulations are used for these sample points to train so-called Gaussian process models, which are widely used in computer experiments for interpolation purposes [24]. The advantage of this method compared with, for example,

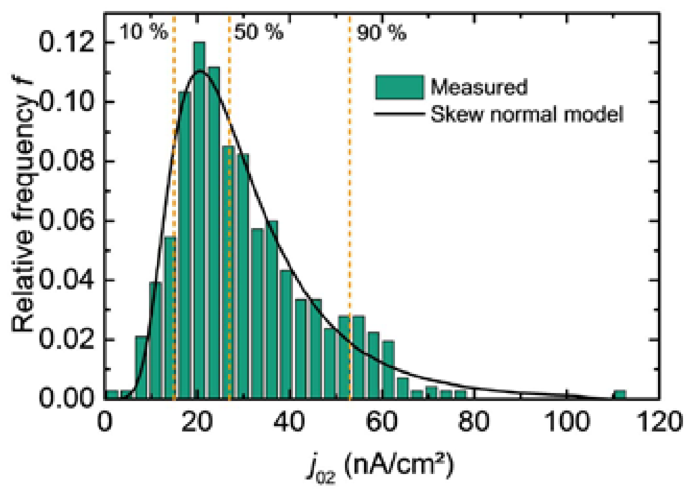

Figure 2. Example of a measured probability density function and the corresponding fitted skew normal model. A good agreement can be seen, despite the use of only three distinct percentiles of the measured distribution for fitting the skew normal model. (Data here taken from a larger experiment.)

polynomial regression is the ability to fit any analytic relationship, including asymptotic trends.

The probability density function of each input parameter is then modelled by fitting the three parameters of a skew normal distribution (Section A.8 in Hosking & Wallis [25]) to the 10th, 50th and 90th percentile of the measured distribution, an example of which is given in Fig. 2. This has the advantage of accounting for the actual inevitable deviations from a strictly symmetric normal distribution. The three distinct percentiles – later referred to as *low*, *medium* and *high* – provide a good estimate of the range of a parameter without being affected by outliers, as would be the case by using, for example, the mean and the variance. Random numbers with values of the order of 10^5 are then drawn from these probability density functions for each input parameter, and the aforementioned Monte Carlo runs (step 4) are performed using the Gaussian process model regression. This lowers the computation time for one simulation of η from 1.5 hours for the numerical simulation to 0.3ms for one Gaussian process model prediction, using one core of a standard CPU.

The resulting modelled distribution of cell efficiencies is then compared with the one obtained experimentally; if necessary, it is adjusted so that all three characteristics j_{sc}, V_{oc} and *FF* simultaneously match the measured ones. If good agreement is achieved, the model is validated and ready for the most interesting part, the final step – 5.

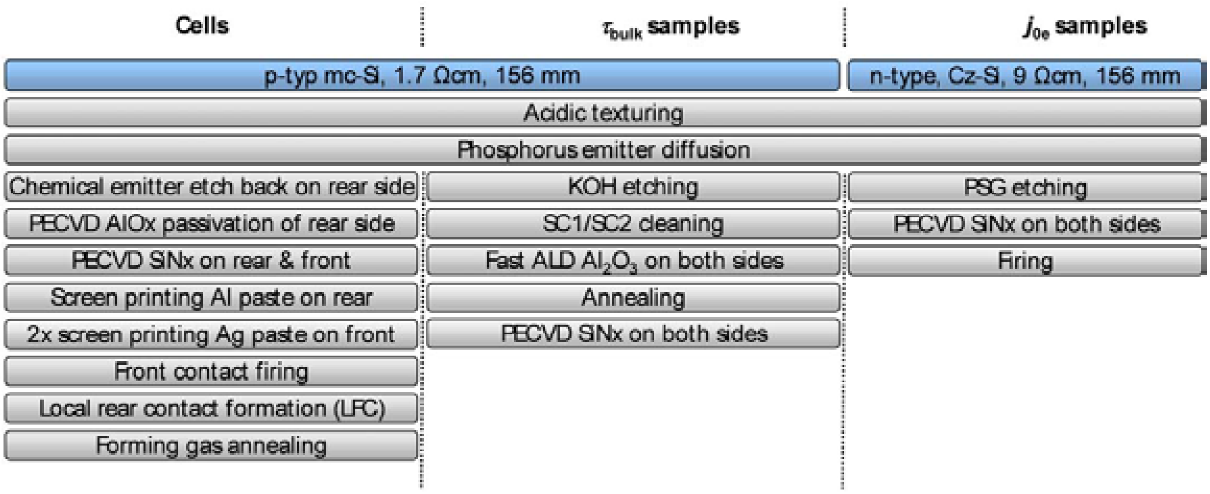

Figure 3. Process flows employed for the cells (left), and for the samples used to measure the bulk lifetime τ_{bulk} (middle) and the emitter dark saturation current density j_{0e} (right).

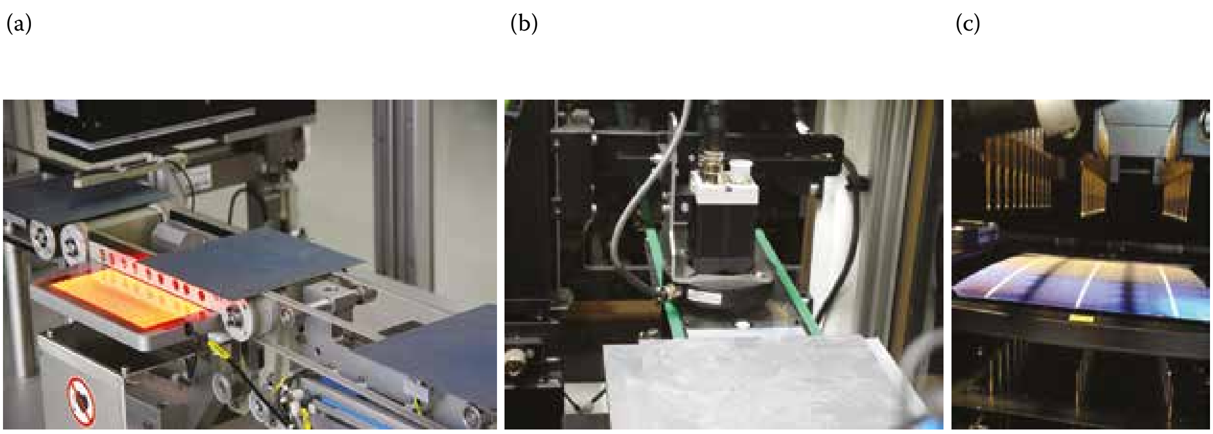

Figure 4. (a) One of the several inline characterization tools available at Fraunhofer ISE's PV-TEC for different stages of the solar cell manufacturing process. (b) Wafer-tracking system based on data matrix codes. (c) State-of-the-art inline automat with a flexible contacting unit, for characterizing the finished cells (which is also suitable for use with back-contact solar cells).

"The variance-based approach takes into account nonlinear responses and considers the interactions between input variables."

Step 5 ultimately features the investigation of the impact of each input parameter on the variations of cell efficiencies in a sensitivity analysis. Variance is a well-established measure of the variation of a random variable; a variance-based approach [26] is therefore chosen for the sensitivity analysis. An advantage of the variance-based approach is its global character, as it takes into account nonlinear responses and considers the interactions between input variables. The principal measure of sensitivity of the total variance V(y) of a random variable y on the input variable x_i is known as the main-effect index S_i and is defined as:

$$S_i = \frac{V(y) - E(V(y|x_i))}{V(y)} = 1 - \frac{E(V(y|x_i))}{V(y)} \tag{1}$$

where V(...) is the variance and E(...) is the mean of a distribution. The term E(V(y|x_i)) is the variance of y when the i_{th} input variable x_i is given (not varied); it is averaged over all possible values of x_i. Thus, S_i is basically a measure of the decrease in total variance V(y) of y when x_i could be fixed and normalized to this total variance. The sum of all the S_i indices is always less than or equal to unity, where a value of unity would indicate an additive model with no interactions between the input variables. Since for the calculation of the S_i one would have to consider distributions of distributions, the short-cut proposed in Saltelli et al. [26] is used, which drastically reduces the computational cost compared with the brute-force method.

Example application

Experimental

The discussed investigation is carried out using an example of an industrially feasible mc-Si PERC process with LFCs, but basically it could be performed on any solar cell concept. In order to be independent of material variations and to gather just the process-related impacts, 51 neighbouring HPM mc-Si wafers are distributed homogeneously among the batches in a larger experiment, so that approximately every 20th cell is processed on this material. It is assumed that the variation in material properties is insignificant over these 51 wafers. An equivalent approach for the production of PERC cells on monocrystalline Czochralski (Cz) grown wafers could be the distribution of high-quality magnetic-cast Cz-Si wafers in the production line.

An essential requirement for this type of study is the possibility of tracking wafers along the entire value chain as far as the finished solar cell, with the use of, for instance, a wafer-tracking system based on data matrix codes [27,28], which has been implemented on Fraunhofer ISE's PV-TEC research manufacturing line.

A flow diagram of the chosen cell process is given in Fig. 3 (left). After the acidic texturing process, the mc-Si base material is subjected to a phosphorus emitter diffusion, using the process developed by Werner et al. [29]. The phosphosilicate glass (PSG) layer on the front side and the emitter on the rear side are then wet-chemically etched back. After a cleaning step, the rear side is passivated by a stack of plasma-enhanced chemical vapour deposited (PECVD) aluminium oxide and silicon nitride, and the front side is passivated by just silicon nitride. Metallization is applied via screen printing, front-contact formation is then achieved with a firing step in a fast-firing conveyor-belt furnace, and the rear side is contacted using the LFC process. After a forming gas annealing step, the cells are characterized inline on a h.a.l.m. cell tester.

In addition to these cells, three of the 51 HPM mc-Si wafers were processed into samples, with the goal of measuring the bulk lifetime τ_{bulk} (process flux depicted in Fig. 3, middle); highly resistive n-type Cz-Si wafers were also processed into samples, to measure the emitter dark saturation current density j_{0e} (Fig. 3, right). For measuring τ_{bulk}, it is important that these samples take part in the same emitter diffusion as the cells in order to account for the impacts of gettering and high-temperature steps on the silicon material; the samples also need to be passivated in the best possible manner. Furthermore, every fifth wafer of the HPM cell material is withdrawn after the deposition of the passivation layers and is subjected to a firing step in a fast-firing oven in order to activate the passivation. These samples for measuring the implied open-circuit voltage iV_{oc} contain valuable information about the front end of the cell process, since they include all recombination effects without any influences due to the metallization.

Data acquisition

During the value chain, the versatile inline and offline characterization methods available at the Photovoltaic Technology Evaluation Center (PV-TEC) at Fraunhofer ISE (see also Fig. 4) are utilized.

The inline methods of the front end prior to metallization consist of the following measurements:

- Wafer thickness d_{Si}, via capacitance.
- Specific resistance ρ of the silicon wafer, via induction.
- Reflectance R_{600nm} at a wavelength of 600nm on a trace of the wafer after texturing, via a spectrometer.
- Imaging of the thickness d_{ARC} of the anti-reflection coating layer, via a hyperspectral imaging sensor.

The base doping concentration N_{dop} is determined by measuring the resistance in the as-cut state; this value is then compared with the one after the emitter etch-back process in order to determine the emitter sheet resistance R_{sh}. In this particular case of an isotexture, the texture strength $\omega_{texture}$ is determined by fitting the simulated R_{600nm} to the measurement after the texturing process, as done by Greulich et al. [15]. The finished cells are then characterized using an inline automat. This allows an inspection of the front and rear side metallization, and the measurement of the metal grid resistance and the current-voltage characteristics under illumination, yielding the performance characteristics j_{sc}, V_{oc}, FF and η, the current–voltage characteristics in the dark, and the suns-V_{oc} characteristics. It also offers the opportunity to record electroluminescence images under forward bias and thermography images under reverse bias. Furthermore, the parallel and series resistances R_p and R_s, as well as the parameters j_{01} and j_{02} by fitting the two-diode model to the suns-V_{oc} pseudo I–V curve, are obtained at the cell level.

The offline methods comprise taking measurements of the spectrally resolved reflectance curves and, using the transfer length method (TLM, [30]), of the metal–semiconductor contact resistance ρ_c of the finished cells. The reflectance curves are used to measure the finger widths and therefore the optical shading ratio M_{met}, by repeated subtraction of the reflectance spectrum of the silver fingers until the expected minimum reflectance of the unmetallized part alone is reached. The parameters R_0 and ω_{Phong} of the Phong model are adjusted to match the measured reflectance of the finished solar cells over the 900–1,200nm wavelength range. The emitter dark saturation current density j_{0e} is determined via a refinement [31] of the Kane-Swanson method [32] applied to quasi-steady-state photoconductance (QSSPC, [33]) measurements of the j_{0e} samples.

Perhaps the most valuable characterization tool is photoluminescence (PL) imaging, the particular use of which here will be described next. PL images at 1 sun are acquired before and after the LFC formation process, and the difference in PL intensities is calibrated to a voltage drop $\Delta V_{oc,LFC}$ because of the additional recombination at the rear contacts. The LFC radius r_{LFC} in the electrical cell simulations is then adjusted to match this voltage drop in the open-circuit voltage V_{oc} [10]. QSSPC lifetime calibrated PL images

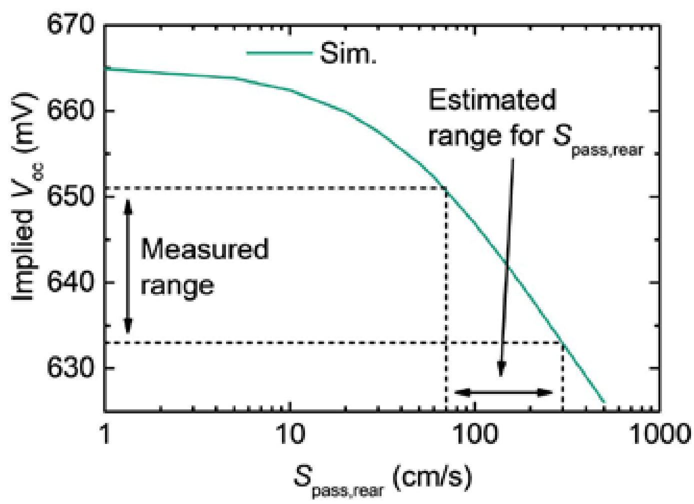

Figure 5. Simulation-assisted estimation of the rear-surface recombination velocity in the passivated area $S_{pass,rear}$ by comparing the measured range of values for the implied open-circuit voltage iV_{oc} with the simulated values.

Parameter	Description	Determination	Low	Medium	High
d_{Si} [µm]*	Bulk thickness	Measurement	183.7	185.4	186.2
N_{dop} [cm^{-3}]	Bulk doping concentration	Measurement	–	9×10^{15}	–
τ_{n0} I τ_{p0} [µs]	Bulk SRH lifetime	τ-calibrated PL of τ_{bulk} samples	–	45 I 910	–
$\omega_{texture}$ [°]	Characteristic texture angle	Adjustments to measured R_{600nm} after texturization	56.5	57.8	61.0
j_{0e} [fA/cm²] I $S_{pass,front}$ [cm/s]	Emitter dark saturation current density	Kane-Swanson method of j_{0e} samples	–	92 I 2.5×10^5	–
$S_{met,front}$ [cm/s]	Recombination velocity at front metallization	Neglected	–	$S_{pass,front}$	–
d_{ARC} [nm]*	ARC layer thickness	Measurement	77.5	79.6	82.2
M_{met} [%]	Shading ratio front metallization	Measurement	5.04	5.36	5.63
$S_{pass,rear}$ [cm/s]	Recombination velocity at rear passivation	Adjustments to measured iV_{oc}	70	130	300
$S_{met,rear}$ [cm/s]	Recombination velocity at rear metallization	Model $S_{met}(N_{dop})$ [19,20]	–	2,400	–
$r_{LFC} = 2r_{LFC,cont.}$ [µm]	Radius of damaged LFC area	Adjustments to measured $\Delta V_{oc,LFC}$	37	44	51
d_{LFC} [µm]	Distance of LFC contacts	LFC target	–	350	–
R_0 [-] I ω [-]	Phong model of reflectance at rear side	Adjustments to measured $R_{>900nm}$ of cell	–	0.935 I 2	
j_{02} [nA/cm²]	Dark saturation current density of second diode	Adjusted two-diode model to pseudo I–V curve	16.5	23.0	34.5
R_s [Ωcm²]	R_s contribution front	Contributions of R_{sh}, ρ_c and R_{grid}	0.523	0.547	0.596

* These parameters are only varied in the optical part of the simulations.

Table 1. Overview of the input parameters, along with their measured ranges and the chosen way of determination. Where just the medium value is given, the parameter variations are neglected in the electrical simulations.

[34] are applied to the samples to measure the implied open-circuit voltage iV_{oc} and the bulk lifetime τ_{bulk}. In the case of the iV_{oc} samples, the lifetime images acquired at 1 sun are converted to images of the local voltage and averaged over the wafer region. As regards the τ_{bulk} samples, an additional image is recorded at 0.04 suns, and the harmonic mean in the diffusion length over the wafer region of the two images is taken; the SRH defect parameters τ_{n0} and τ_{p0}, required as simulation input to fit the lifetime values at the two different injection conditions, are then adjusted. Along with the use of the measured j_{0e} and τ_{bulk}, the surface recombination velocity $S_{pass,rear}$ of the passivated area where the damaged LFC area is absent is varied in cell simulations, in order to match the measured range of iV_{oc}, as depicted in Fig. 5, and to determine $S_{pass,rear}$.

In order to reproduce in the model the measured dark saturation current densities $j_{02,fit}$ derived from the measured I–V curves with the simulations, the difference $j_{02} = j_{02,fit} - j_{02,Sent.Device}$, where $j_{02,Sent.Device}$ is obtained by fitting the two-diode model to an example Sentaurus Device I–V curve, is used as the saturation current density of the external second diode. Finally, the series contribution R_s of the front is calculated by area weighting the single contributions of emitter sheet resistance R_{sh}, specific contact resistance ρ_c and grid resistance R_{grid}.

An overview of the input parameters, along with their measured ranges and the chosen method of determination, is given in Table 1. Compared with a previous study, the absolute values of τ_{n0}, M_{met} and j_{02} are slightly different, but the absolute ranges of these variables remain the same. This is acceptable, since it is primarily the variations in cell efficiencies that are of interest.

"The rear-surface recombination velocity in the passivated area is the dominant origin of efficiency variations."

Results

The experimentally obtained distribution of cell efficiencies and the modelled one are given in Fig. 6(a): excellent agreement in both the absolute level and the shape is seen. Note that the solar cells with severe series and parallel resistance issues, represented by the leftmost bar on the chart, were removed prior to determining the mean and the standard deviation. The total standard deviation of the conversion efficiency η in the experiment amounts to 0.23%$_{abs.}$, and more than 80% of the closely related variance in the simulations can be explained. The results of the variance-based sensitivity analysis are given in Fig. 6(b), which shows a breakdown of the various influences. The sum of the aforementioned main-effect indices S_i, which serve as sensitivity measures, turns out to be equal to unity within the uncertainties that are due to statistical computation, clearly indicating an additive model $\eta(x_1,\ldots,x_n)$. It is therefore possible to assign a relative share of the total variance to each of the input parameters x_i, revealing that the rear-surface recombination velocity in the passivated area S_{pass} is the dominant origin of variations. Further technological work should focus on improving the stability and the overall quality of the rear-surface treatment and cleaning, and the PECVD of the passivation.

The large process-induced j_{02} contribution is the second-largest source and is responsible for more than a third of the variation in η. This contribution can be attributed to power losses at the wafer edges, which is underlined by the dark lock-in thermography (DLIT) image at +0.5V for a cell with severe pseudo fill factor problems, shown in Fig. 7. At these distinct edges, a wrap-around of liquid during the emitter etch-back process was visible, even to the naked eye. Subsequent finger printing and firing most likely resulted in the formation of recombination-active defects in the depletion region between the partially etched emitter and the base. For the PERC process utilized, after an optimization of the rear-surface passivation and chemical edge isolation processes (which are responsible for over 80% of the process-induced variations), the next steps to be recommended would include improvements to the optics of the

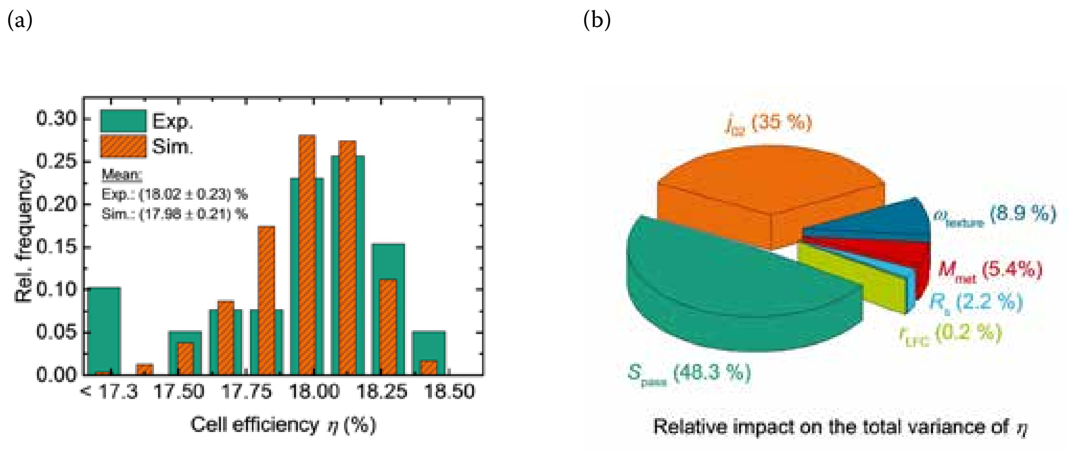

Figure 6. (a) Experimentally obtained (green) and modelled (orange) distributions of cell efficiencies. Prior to determining the mean and the standard deviation in the experiment, the cells with severe series and parallel resistance problems (leftmost bar on the chart) were excluded and a skew normal distribution fitted to the remaining data. (b) Pie chart of the ranked relative impacts of each input parameter on the total variance of cell efficiencies. The variation in rear-surface recombination is the dominant source of variations in energy conversion efficiency η.

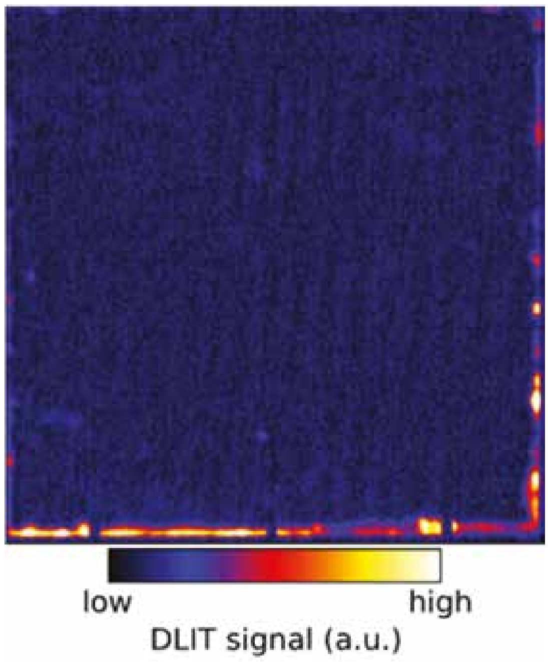

Figure 7. Dark lock-in thermography (DLIT) image at +0.5V of a cell with severe pseudo fill factor problems (pFF = 77.7%, j_{02} = 65nA/cm², R_p = 5,162Ωcm²). The power loss which is clearly visible at the bottom and right cell edges was found to be caused by a wrap-around of liquid during the emitter etch-back process. Subsequent finger printing and firing most likely led to the formation of recombination-active defects in the depletion region between the partially etched emitter and the base.

front side, namely the texture strength ω_{texture} and the front metallization shading ratio M_{met}.

> "The parameters that lead to the largest variations are often the same ones that offer the greatest potential for optimizing the absolute level of cell efficiencies."

Conclusions

A simulation-based approach for modelling the experimentally obtained distribution of solar cell efficiencies has been introduced. It was shown how to rank the input parameters according to their influence on the total variance of this distribution, thus giving an indication of which processes and parameters need to be measured and better tuned. This approach was illustrated and verified using an example of an industrially feasible mc-Si PERC process with LFC contacts, for which it was possible to explain over 80% of the measured efficiency variation of 0.23%$_{\text{abs.}}$. In this case, the rear-surface passivation and a wrap-around during the emitter etch-back process were identified to be responsible for 80% of the efficiency variation. These two processes should therefore be the first to be optimized in the PERC manufacturing process utilized.

This sensitivity analysis can be transferred to other production lines and cell concepts. It is especially helpful for ramping up, for example, PERC production, but can also be used for improving a currently operating production line, since the parameters that lead to the largest variations are often the same ones that offer the greatest potential for optimizing the absolute level of cell efficiencies. Not only is the presented approach basically applicable to every type of solar cell concept, but it can also contribute valuable information towards improving the quality and the yield of any production line, and consequently help in increasing the cost-effectiveness of solar cell manufacturing.

Acknowledgements

The experiments discussed in this paper were conducted under the framework of the 'Q-Wafer' Project (03SF0409A and B), supported by the German Ministry for Education and Research (BMBF). The authors would like to thank all the team at PV-TEC who helped in the processing and characterization segments, and made this work possible. Sven Wasmer gratefully acknowledges the support by scholarship funds from the State Graduate Funding Program of Baden-Württemberg. Nico Wöhrle gratefully acknowledges the scholarship from the German Federal Environmental Foundation ('Deutsche Bundesstiftung Umwelt').

References

[1] SEMI PV Group Europe 2015, "International technology roadmap for photovoltaic (ITRPV): 2014 results", 6th edn (Apr.), Revision 1 (Jul.) [http://www.itrpv.net/Reports/Downloads/].

[2] Blakers, A.W. et al. 1989, "22.8% efficient silicon solar cell", *Appl. Phys. Lett.*, Vol. 55, No. 13, pp. 1363–1365.

[3] Greulich, J. et al. 2013, "Numerical power balance and free energy loss analysis for solar cells including optical, thermodynamic, and electrical aspects", *J. Appl. Phys.*, Vol. 114, No. 20, p. 204504.

[4] Evans, R. et al. 2014, "Data mining photovoltaic cell manufacturing data", *Proc. 40th IEEE PVSC*, Denver, Colorado, USA, pp. 2699–2704.

[5] Evans, R. et al. 2014, "Interpreting manufacturing variance using a data mining approach", *Proc. 29th EU PVSEC*, Amsterdam, The Netherlands, pp. 406–411.

[6] Evans, R. et al. 2015, "Multivariate analysis of wafer process data", *Proc. 31st EU PVSEC*, Hamburg, Germany, pp. 912–917.

[7] Fischer, G. et al. 2012, "A combined statistical and TCAD model as a method for understanding and reducing variations in multicrystalline Si solar cell production", *Energy Procedia*, Vol. 27, pp. 203–207.

[8] Müller, M. et al. 2013, "Understanding and reducing the variations in multicrystalline Si solar cell production", *Proc. 28th EU PVSEC*, Paris, France, pp. 867–871.

[9] Müller, M. et al. 2014, "Sensitivity analysis of industrial multicrystalline PERC silicon solar cells by means of 3-D device simulation and metamodeling", *IEEE J. Photovolt.*, Vol. 4, No. 1, pp. 107–113.

[10] Wasmer, S. et al. 2015,

"Investigating the impact of parameter and process variations on multicrystalline silicon PERC cell efficiency", *Proc. 31st EU PVSEC*, Hamburg, Germany, pp. 477–484.

[11] Synopsis 2013, Sentaurus TCAD.

[12] Schneiderlöchner, E. et al. 2001, "Laser-fired contacts (LFC)", *Proc. 17th EU PVSEC*, Munich, Germany, pp. 1303–1306.

[13] Macleod, H.A. 2001, *Thin-film Optical Filters*. Boca Raton, FL: Taylor & Francis.

[14] Baker-Finch, S.C., McIntosh, K.R. & Terry, M.L. 2012, "Isotextured silicon solar cell analysis and modeling 1", *IEEE J. Photovolt.*, Vol. 2, No. 4, pp. 457–464.

[15] Greulich, J. et al. 2015, "Optical simulation and analysis of iso-textured silicon solar cells and modules including light trapping", *Proc. 5th SiliconPV Conf.*, Konstanz, Germany, pp. 69–74.

[16] Hecht, E. 2002, *Optics*. Toronto: Addison-Wesley Longman.

[17] Phong, B.T. 1975, "Illumination for computer generated pictures", *Commun. ACM*, Vol. 18, No. 6, pp. 311–317.

[18] Rüdiger, M. & Hermle, M. 2012, "Numerical analysis of locally contacted rear surface passivated silicon solar cells", *Jpn. J. Appl. Phys.*, Vol. 51, p. 10NA07.

[19] Schwab, C. 2013, "Herstellung und Charakterisierung industrieller oberflächenpassivierter p-typ Solarzellen", Dissertation, Fraunhofer ISE, Albert Ludwig University, Freiburg, Germany.

[20] Wöhrle, N. et al. 2014, "Efficiency potential simulation for an industrially feasible LFC-PERC concept with sensitivity analysis on crucial cell parameters", *Proc. 29th EU PVSEC*, Amsterdam, The Netherlands, pp. 421–426.

[21] Fell, A. et al. 2015, "Input parameters for the simulation of silicon solar cells in 2014", *IEEE J. Photovolt.*, Vol. 5, No. 4, pp. 1250–1263.

[22] Altermatt, P. 2011, "Models for numerical device simulations of crystalline silicon solar cells – a review", *J. Computat. Electron.*, Vol. 10, No. 3, pp. 314–330.

[23] MacCalman, A.D. 2012, DesignCreatorv2 Spreadsheet.

[24] Sacks, J. et al. 1989, "Design and analysis of computer experiments", *Statist. Sci*, pp. 409–423.

[25] Hosking, J.R.M. & Wallis, J.R. 2005, *Regional Frequency Analysis: An Approach Based on L-moments*. Cambridge, UK: Cambridge University Press.

[26] Saltelli, A. et al. 2010, "Variance based sensitivity analysis of model output: Design and estimator for the total sensitivity index", *Computat. Phys. Comm.*, Vol. 181, No. 2, pp. 259–270.

[27] Wanka, S. et al. 2011, "Tra.Q – Laser marking for single wafer identification – Production experience from 100 million wafers", *Proc. 37th IEEE PVSC*, Seattle, Washington, USA, pp. 1101–1104.

[28] Krieg, A., Rajsrima, N. & Rein, S. 2011, "Laser marking of solar cells: Technologies and potential", *Proc. 26th EU PVSEC*, Hamburg, Germany, pp. 2130–2134.

[29] Werner, S. et al. 2014, "Process optimization for the front side of p-type silicon solar cells", *Proc. 29th EU PVSEC*, Amsterdam, The Netherlands, pp. 1342–1347.

[30] Mak, L.K., Rogers, C.M. & Northrop, D.C. 1989, "Specific contact resistance measurements on semiconductors", *J. Phys. E: Sci. Instrum.*, Vol. 22, No. 5, pp. 317–321.

[31] Kimmerle, A., Greulich, J. & Wolf, A. 2015, "Carrier-diffusion corrected J_0-analysis of charge carrier lifetime measurements for increased consistency", *Sol. Energy Mater. Sol. Cells*, Vol. 142, pp. 116–122.

[32] Kane, D.E. & Swanson, R.M. 1985, "Measurement of the emitter saturation current by a contactless photoconductivity decay method (silicon solar cells)", *Proc. 18th IEEE PVSC*, Las Vegas, Nevada, USA, pp. 578–583.

[33] Sinton, R.A., Cuevas, A. & Stuckings, M. 1996, "Quasi-steady-state photoconductance, a new method for solar cell material and device characterization", *Proc. 25th IEEE PVSC*, Washington DC, USA, pp. 457–460.

[34] Giesecke, J.A. et al. 2011, "Minority carrier lifetime of silicon solar cells from quasi-steady-state photoluminescence", *Sol. Energy Mater. Sol. Cells*, Vol. 95, No. 7, pp. 1979–1982.

About the Authors

Sven Wasmer studied physics at the University of Freiburg, Germany, and received his diploma in 2013 in collaboration with Fraunhofer ISE, Freiburg. He is currently working towards his Ph.D. at Fraunhofer ISE on the characterization and simulation of process variations in solar cell production.

Johannes Greulich studied physics in Heidelberg and in Freiburg, Germany, and obtained his diploma in 2010. In 2014 he received a Ph.D. in physics from the University of Freiburg for his work on simulation and characterization of novel large-area silicon solar cells. Since 2015 he has headed a research team at ISE working on inline solar cell characterization, device simulation and image processing.

Hannes Höffler received his diploma in physics in 2010 from the University of Freiburg, Germany. In 2015 he obtained a Ph.D. in physics from the University of Freiburg for his work on luminescence imaging and its applications in an industrial silicon solar cell processing environment. He is currently responsible for the offline characterization laboratory in the production technology and quality assurance division at Fraunhofer ISE.

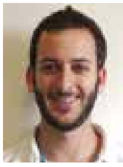

Nico Wöhrle studied physics at the University of Freiburg, Germany, and received his diploma in 2011 in collaboration with Fraunhofer ISE, Freiburg. He is currently finishing his Ph.D. at Fraunhofer ISE, with a thesis specialization in solar cell device simulation and loss analysis of silicon solar cells.

Stefan Rein is head of the inline measurement techniques and laser process technologies/quality assurance group at Fraunhofer ISE. He studied physics at the Albert Ludwig University of Freiburg and received his diploma degree in 1998. He was awarded a Ph.D. in 2004 for his work on lifetime spectroscopy for defect characterization in silicon for PV applications, carried out at Fraunhofer ISE.

Enquiries

Sven Wasmer
Fraunhofer ISE
Heidenhofstraße 2
79110 Freiburg
Germany

Tel: +49 (0)761 4588 5012
Email: sven.wasmer@ise.fraunhofer.de